CONFERENCE PRE-PRINT

A NOVEL COMPUTATION OF THE LINEAR PLASMA RESPONSE TO A RESONANT ERROR FIELD IN SINGLE FLUID VISCO-RESISTIVE MHD AND APPLICATION TO THE RFX-MOD2 TOKAMAK

P. ZANCA

Consorzio RFX (CNR, ENEA, INFN, Università di Padova, Acciaierie Venete SpA) Padova, Italy

Email: paolo.zanca@igi.cnr.it

L. MARRELLI

Consorzio RFX (CNR, ENEA, INFN, Università di Padova, Acciaierie Venete SpA). Istituto per la Scienza e la Tecnologia dei Plasmi (ISTP), CNR Padova, Italy

D. TERRANOVA

Consorzio RFX (CNR, ENEA, INFN, Università di Padova, Acciaierie Venete SpA). Istituto per la Scienza e la Tecnologia dei Plasmi (ISTP), CNR Padova, Italy

Abstract

Dynamical simulations of error field (EF) penetration in a tokamak plasma are performed in cylindrical geometry. This is accomplished by the RFX-locking code, already used to simulate the tearing mode dynamic in tokamaks [L. Piron et al, Nucl. Fusion **64** 066029 (2024).]. To this purpose, the code is enriched by recently developed specific physics describing the linear plasma response to a resonant EF [P. Zanca, Nucl. Fusion **65** 056023 (2025)]. Application to cylindrical proxy of JET and RFX-mod2, the revamped RFX-mod experiment, are discussed.

1. INTRODUCTION

Magnetic confinement experiments are inevitably subject to error fields (EF), namely small amplitude static magnetic fields due to coils and machine imperfections. They represent a concern when they resonate in the plasma, namely when they have the same helicity as the equilibrium field at a given radius (resonant surface). In this case, EF drives magnetic reconnection in intrinsically tearing-stable plasmas, and above an amplitude threshold it produces a wall locked magnetic island, making the plasma prone to a disruption. This phenomenon is known as error-field penetration. A research line interprets EF penetration with linear magneto-hydrodynamic (MHD), in both one fluid and two-fluids (drift-MHD) versions [1, 2, 3, 4]. The justification for using linear theory is that plasma rotation suppresses the EF driven reconnection before the penetration takes place. The linear plasma response is encapsulated within the delta prime (Δ '), a quantity which measures the magnitude and phase of the current sheet induced by the plasma rotation at the resonant surface, shielding the EF penetration. Recently, a new Δ' computation in single-fluid MHD has been presented [5]. That work re-examines the problem from the very beginning, giving a better justification of the mathematical techniques usually adopted in this context. Moreover, it provides a reliable solution method more general than the asymptotic-regimes techniques elsewhere proposed [1]. The generalization of this method to the two-fluids drift-MHD is developed in a further paper [6]: with respect to the previous single-fluid computation [5] no significant difference in the EF threshold is found for ohmic plasma conditions. Therefore, in the present work we will limit to the single fluid model. In two mentioned analyses [5, 6] the EF penetration threshold is estimated by a steady state analysis. Instead, here we provide dynamical simulation of the EF penetration process. To this purpose, the Δ' computation developed in [5] is included in the cylindrical RFX-locking code. This code was initially written for modelling the tearing modes dynamics in the reversed-field-pinch [7], but it was subsequently adapted to the tokamak case [8, 9]. Two devices will be simulated: a cylindrical proxy of JET and a cylindrical proxy of RFX-mod2 [10, 11], the revamped RFX-mod experiment, which is predicted to start operations in the next years. The paper is organized as follows. In section 2 the model is presented. In section 3 the simulations are discussed. Section 4 draws the conclusions.

THE MODEL

The present study is performed with the cylindrical RFX-locking code. The formalism used in the code derives to a large extent from [1], and it is based on a reduction of the single-fluid, visco-resistive MHD equations with zero pressure gradient, in cylindrical geometry. We also mention a recent application to ITER of a similar model [12]. We describe the plasma as a cylindrical configuration with periodicity length $2\pi R_0$ in the z direction: R_0 is the simulated plasma major radius, and the minor radius is denoted by a. We adopt the coordinates $(r, \theta, \phi = z/R_0)$, and we exploit the force-free condition $\nabla \times \boldsymbol{B_0} = \mu_0 \boldsymbol{J_0} = \sigma(r) \boldsymbol{B_0}$, with $\sigma(r)$ an input function, to determine the equilibrium magnetic field $\boldsymbol{B_0} = (0, B_{0\theta}, B_{0\phi})$. The Fourier harmonics of a generic perturbed quantity are defined by the series $X(r, \theta, \phi, t) = \sum_{m,n \in \mathbb{Z}} x^{m,n} (r, t) e^{i(m\theta - n\phi)}$. The model's equations can be grouped into four categories, described in following paragraphs. The first deals with the so-called 'outer region', which consists of the most part of the plasma and the vacuum region: here, we limit to the ideal-MHD description at the leading order in the perturbation, though viscosity is included at the second order to model the velocity profile evolution. The second category deals with the so-called 'inner region', namely a radially thin portion of plasma about the resonant surface: in this region all the terms of the original visco-resistive equations are retained. The third category concerns the passive and active conductive structures surrounding the plasma. Finally, the fourth category specifies some important kinetic quantities entering the above equations.

2.1. Outer region

In most of the plasma and vacuum regions, the radial profile of the magnetic perturbation produced by a (m, n) EF can be described by the ideal-MHD, force-balance equation, linearized in the perturbation (Newcomb's equation) [13]:

1)
$$\frac{\partial}{\partial r} \left(\frac{r}{H_{mn}} \frac{\partial}{\partial r} \psi^{m,n} \right) - \left[\frac{1}{r} + \frac{r G_{mn}}{H_{mn} F_{mn}} \frac{d\sigma}{dr} + \frac{2 m n \varepsilon \sigma}{H_{mn}^2} - \frac{r \sigma^2}{H_{mn}} \right] \psi^{m,n} = 0$$

2)
$$\psi^{m,n}(r,t) = -i r b_r^{m,n}(r,t)$$

3)
$$\varepsilon(r) = r/R_0$$
, $H_{mn}(r) = m^2 + n^2 \varepsilon^2$, $G_{m,n} = mB_{0\phi} + n\varepsilon B_{0\theta}$, $F_{m,n} = mB_{0\theta} - n\varepsilon B_{0\phi}$

Equation (1), which is at the first order in the perturbation, is singular at the resonant surface, identified by the radius $r_{m,n}$ such that $F_{m,n}(r_{m,n})=0$. Therefore, it is solved in the separate regions $0 < r < r_{m,n}$ and $r > r_{m,n}$, by imposing the continuity of $\psi^{m,n}$ at $r=r_{m,n}$. The singularity is resolved by a detailed analysis in a narrow region around $r_{m,n}$ (inner region), which includes non-ideal physics. This will be shown in the next paragraph. In general, the radial derivative of $\psi^{m,n}$ is discontinuous at $r=r_{m,n}$: this fact marks the presence of a current sheet localized at the resonant surface. The mode at the resonant surface is denoted by the symbol $\Psi^{m,n}_s \equiv \psi^{m,n}(r_{m,n},t)$. Hereafter, we will drop the superscript (m,n), unless when strictly necessary.

Plasma viscosity enters the motion equation at the second order in the perturbation, in order to evolve the toroidal and poloidal angular velocities averaged over the angular co-ordinates, $\Omega_{\phi}(r,t)$, $\Omega_{\theta}(r,t)$:

4)
$$\rho \frac{\partial}{\partial t} \Omega_{\phi} = \frac{\rho a^2}{\tau_V} \frac{1}{r} \frac{\partial}{\partial r} \left(r \frac{\partial}{\partial r} \Omega_{\phi} \right) + S_{\phi} + \frac{1}{4\pi^2 r R_3^3} T_{EM,\phi} \delta(r - r_{m,n})$$

5)
$$\rho \frac{\partial}{\partial t} \Omega_{\theta} = \frac{\rho a^2}{\tau_V} \frac{1}{r^3} \frac{\partial}{\partial r} \left(r^3 \frac{\partial}{\partial r} \Omega_{\theta} \right) - \frac{\rho}{\tau_{\theta}} \Omega_{\theta} + S_{\theta} + \frac{1}{4\pi^2 r^3 R_0} T_{EM,\theta} \delta \left(r - r_{m,n} \right)$$

 ρ is the mass density, τ_V is the diffusion time associated to the perpendicular viscosity, τ_θ is the neoclassical poloidal flow damping time, and S_ϕ , S_θ are phenomenological momentum sources. For the sake of simplicity all these quantities are taken constant with r. The terms $\Omega_\theta/\tau_\theta$, S_ϕ , S_θ are included ad hoc. $T_{EM,\phi}$, $T_{EM,\theta}$ are the toroidal and poloidal components of the electromagnetic (EM) torque integrated over the angular coordinates, which develops near the resonant surface due to the $J \times B$ term taken at the second order in the perturbations. The Dirac delta models the local radial character of the EM torque. Indeed, at the resonant surface the static EF induces both a current sheet, mainly as a consequence of the plasma rotation (in the plasma frame of reference EF is seen rotating), and a non-zero radial field, as a consequence of the partial reconnection (partial because it is hindered by the current sheet). The coupling between these two effects gives rise to an electromagnetic torque T_{EM} in the vicinity of the resonant surface. This torque can be modelled by standard quasi-linear expressions as reported in [7, 13]:

6)
$$T_{EM,\phi} = \frac{8\pi^2 R_0}{\mu_0} \frac{n \, r_{mn}}{H_{mn}} |\Psi_s|^2 Im(\Delta'), \qquad T_{EM,\theta} = -m/n \, T_{EM,\phi}$$

The so-called delta-prime parameter Δ' , defined by

7)
$$\Delta' = \frac{1}{\Psi_s} \frac{d}{dr} \psi^{m,n} \Big|_{r_{m,n}-}^{r_{m,n}+}$$

is the normalized radial field derivative discontinuity at the resonant surface. Therefore, $\Psi_s\Delta'$ quantifies amplitude and phase of the current sheet. Formula (6) can be understood in this way: $i\Psi_s$ quantifies the radial field at the resonant surface, $\Psi_s\Delta'$ quantifies the current sheet, so that the real part of the product $\Psi_s\Delta'$ ($i\Psi_s$)* gives the angular integrated electromagnetic torque.

We can express Ψ_s in terms of Δ' and the perturbation at the vacuum vessel $\Psi_v \equiv \psi(r_v, t)$ (the plasma-facing structure; see paragraph 2.3) by the following relationship [5]

8)
$$\Psi_{s} = \frac{E_{vs} \Psi_{v}}{r_{mn} \Delta' - E_{s}}, \quad E_{s} = r \frac{d}{dr} \hat{\psi}_{s} \Big|_{r_{m,n}}^{r_{m,n}}, \quad E_{vs} = r \frac{d}{dr} \hat{\psi}_{v} \Big|_{r_{m,n}}^{r_{m,n}}$$

The real dimensionless parameters E_s , E_{vs} are the radial derivative discontinuities respectively of the Newcomb's equation solution $\hat{\psi}_s$ which is 1 at $r_{m,n}$ regular in the origin, and zero at $r=r_v$, and of the solution $\hat{\psi}_v$ which is 1 at $r=r_v$ and zero for $r \leq r_{m,n}$. They are fixed by the magnetic equilibrium and by the plasma-vessel proximity. Relation (8) derives from (7) and from identity $r\frac{d}{dr}\psi^{m,n}\Big|_{r_{m,n}}^{r_{m,n}+}=E_s\Psi_s+E_{vs}\Psi_v$. We take the function $\sigma(r)$, which specifies the equilibrium, in order to make the plasma stable to tearing modes in the absence of EF ($\Psi_v=0$): this requires $E_s<0$ [14].

2.2. Inner region

The purpose of the inner region analysis is computing Δ' in terms of plasma parameters such as rotation velocity, resistivity and viscosity. We adopt the novel method presented in [5] to derive Δ' in the single-fluid visco-resistive MHD. For the details we refer to that paper, whereas here we limit to the main results. The single-fluid ohm's law and motion equation are retained in full in the inner region:

9)
$$\mathbf{E} + \mathbf{V} \times \mathbf{B} = \eta \mathbf{J}$$

10)
$$\rho\left(\frac{\partial}{\partial t} + \boldsymbol{V} \cdot \nabla\right) \boldsymbol{V} = \boldsymbol{J} \times \boldsymbol{B} + \frac{\rho a^2}{TV} \nabla^2 \boldsymbol{V}$$

 η is the plasma resistivity, taken radially constant. Equations (9), (10) are analysed in slab cartesian geometry, suitable to the narrow inner region. Moreover, we take quasi-stationary conditions ($\partial/\partial t \cong 0$), since the EF is assumed static, so the induced modifications on magnetic field and velocity slowly evolve. After a normalization and a reduction process, which includes the expression of V in terms of a stream function ϕ by $V = \nabla \phi \times \hat{z} + V_z \hat{z}$, equations (9), (10) provide the following two linear equations for the normalized magnetic perturbation harmonic $\tilde{\psi}$ and the normalized perturbation harmonic $\tilde{\phi}$ of the velocity stream function:

11)
$$\frac{d^2\tilde{\psi}}{dX^2} = iQ \ \tilde{\psi} - iX \ \tilde{\phi},$$
 $X = S^{1/3} (r - r_{m,n})/r_{m,n},$ $S = \tau_R/\tau_A,$ $Q = S^{1/3}\tau_A\omega$

12)
$$X \frac{d^2 \widetilde{\psi}}{dX^2} = Q \frac{d^2 \widetilde{\phi}}{dX^2} + i P \frac{d^4}{dX^4} \widetilde{\phi}, \qquad P = \tau_R / \tau_V$$

 $S\gg 1$ and P are respectively the Lundquist number and the Prandtl number, with τ_A the Alfven time, and $\tau_R=\mu_0a^2/\eta$ the resistive diffusion time, respectively; X is a normalized radial stretched variable, with $X\to\pm\infty$ corresponding to the boundary of the inner region; $\omega=m\Omega_\theta(r_{m,n})-n\Omega_\phi(r_{m,n})$ is the EF frequency as seen by the frame co-rotating with the plasma at the resonant surface. Note that Q is a normalized EF frequency. Then, Δ' is computed from the asymptotic behaviour for $X\to\pm\infty$ of the solution of (11), (12). As shown in [5], the most

efficient method to solve (11), (12) involves the Fourier transform of the same equations by defining $\bar{\phi}(k) = \int_{-\infty}^{+\infty} \tilde{\phi}(X) e^{-ikX} dX$, $\bar{\psi}(k) = \int_{-\infty}^{+\infty} \tilde{\psi}(X) e^{-ikX} dX$:

13)
$$(k^2 + iQ)\bar{\psi} + \frac{d}{dk}\bar{\phi} = 0$$
, $i\frac{d}{dk}(-k^2\bar{\psi}) + (Qk^2 - iPk^4)\bar{\phi} = 0$

The eligibility of the Fourier transform as a technique for solving (11), (12) has been justified in [5]. Then equations (13) are combined to get the single equation for $\bar{\phi}$

14)
$$\frac{d}{dk} \left[\frac{k^2}{k^2 + iQ} \frac{d}{dk} \bar{\phi} \right] = k^2 (iQ + Pk^2) \bar{\phi}$$

which should be solved by imposing the vanishing of $\bar{\phi}$ at $k \to \infty$. We circumvent the problem of assigning the correct boundary condition to $\bar{\phi}$ at infinity, by taking the Riccati transformation [15] $\bar{w}(k) = k^2/(k^2 + iQ) d\bar{\phi}/dk/\bar{\phi}$, to get the following first-order non-linear equation in \bar{w} :

15)
$$\frac{d}{dk} \overline{w} + \frac{k^2 + iQ}{k^2} \overline{w}^2 = k^2 (iQ + Pk^2)$$

This equation is numerically integrated backward from k_{max} to 0: the solution quickly becomes insensitive to the initial condition $\overline{w}(k_{max})$, since the behavior at $k \to 0$ is fixed by $\overline{w}(k) = ik/Q + o(k^2)$ and the equation is of the first order. Δ' is then extracted from the asymptotic behavior of $\overline{w}(k)$ at $k \to 0$, which indeed corresponds to the behavior at $X \to \pm \infty$ of the original fields $\widetilde{\psi}(X)$, $\widetilde{\phi}(X)$.

2.3. Conductive structures

The solution of (1) is matched with the solutions of specific equations modelling the active and passive conductive structures, placed in the region r > a. The plasma is surrounded by a vacuum vessel at the radius $r_v > a$, approximated by a uniform shell with infinitesimal thickness and time constant τ_v . The evolution of the magnetic perturbation across the vessel is ruled by the thin-shell equation derived in [16]:

16)
$$\tau_v \frac{\partial}{\partial t} \psi(r_v) = r_v \frac{d}{dr} \psi \Big|_{r_v - r_v}^{r_v + r_v}$$

The discontinuity in the right-hand-side of (16) is produced by the image currents, which develop onto the vessel. Outside the vessel, we place a thick support structure modelled by a uniform shell placed at the radius $r_b > r_v$, with thickness δ_b , electrical conductivity σ_b and time constant $\tau_b = \mu_0 r_b \delta_b \sigma_b$. The evolution of the perturbation inside the structure is approximated by the diffusion equation derived in [16] too:

17)
$$\tau_b \frac{\partial}{\partial t} \psi = r_b \, \delta_b \frac{\partial^2}{\partial r^2} \psi, \qquad r_b \le r \le r_b + \delta_b$$

A $M_c \times N_c$ grid of identical, evenly spaced rectangular coils, with M_c , N_c the numbers in the poloidal and toroidal directions respectively, is placed outside the support structure at $r_c > r_b$. The uniform grid defines the current harmonics by

18)
$$I_c^{m,n} = \frac{1}{M_c N_c} \sum_{i=1, M_c} I_{k,j} e^{-i(m\theta_k - n\phi_j)}$$

with $I_{k,j}$ the coils' currents and θ_k , ϕ_j the poloidal and toroidal angles of the coils, respectively. The (m,n) EF is *artificially* produced by a current harmonic $I_c^{m,n} \neq 0$. This harmonic produces the following discontinuity in the radial derivative of $\psi^{m,n}$ at the coils radius:

19)
$$r_c \frac{d}{dr} \psi^{m,n} \Big|_{r_c-}^{r_c+} = i L_c^{m,n} I_c^{m,n}, \qquad L_c^{m,n} = \mu_0 [m^2 + (n r_c / R_0)^2] f_c(m,n)$$

with f_c a shape factor. If the coils' conductor thickness is much smaller than r_c , we can adopt the approximation $f_c(m,n) \cong sin(m \Delta\theta_c/2)/(m \Delta\theta_c/2) \times sin(n \Delta\phi_c/2)/(n \Delta\phi_c/2)$ [17], with $\Delta\theta_c$, $\Delta\phi_c$ the poloidal and toroidal angular extent of the coils.

2.4. Some kinetic quantities

As far as the kinetic quantities are concerned, we adopt the same definition used in the analysis of the ohmic tokamak presented in [6]. The reason for considering the ohmic tokamak is that scaling laws of the electron and ion temperatures, which enter in several parameters of the model, are available in this configuration. From [18] we take the following expression for the on-axis electron temperature (SI units are used, apart from the temperature given in keV):

20)
$$T_{e0}(keV) \approx Exp(-12)a^{-1.24}R_0^{0.97}I_p^{0.81}Z_{eff}^{0.37}$$

 I_p is the plasma current, and Z_{eff} the plasma effective charge. Several scaling laws for the ion temperature have been proposed in the early ohmic tokamaks [19]. Here, we take the Artsimovitch's expression T_{iA} [20] corrected by a factor coming from the energy exchange with electrons

21)
$$T_{i0}(keV) = T_{iA} \times \left(\frac{f}{0.338}\right)^{1/3}$$
, $f = \frac{\frac{T_{e0}}{T_{i0}} - 1}{\left(\frac{T_{e0}}{T_{i0}}\right)^{3/2}}$, $T_{iA}(keV) \approx 1.29 \times \left[I_p(MA) B_{0\phi} n(10^{20}) R_0^2\right]^{1/3} A_i^{-1/2}$

 A_i is the mass number. Expression (21) is an equation for T_{i0} , with T_{e0} as input. The expression for T_{iA} is compatible with gyro-Bohm ion thermal diffusivity [6]. As far as the temperature profile is concerned, we take a parabola for both ions and electrons, The viscous diffusion time τ_V is proportional to the momentum confinement time τ_M defined as the ratio of the total toroidal angular momentum to the toroidal angular momentum input. Here we take $\tau_V = \tau_M$. JET analyses show a good correlation of τ_M with the ion energy replacement time τ'_{Ei} [21], suggesting the identification $\tau_M = \tau'_{Ei}$. The latter is computed by

$$22) \ \tau'_{Ei} \approx \frac{3}{2} \frac{n \left(10^{20}\right) \langle T_i \rangle \times 1.6 \times 10^4}{q_{ei}}, \quad \ q_{ei} \approx 4.33 \times 10^8 \frac{m_e}{m_i} Z_i \ ln \Lambda \ n^2 (10^{20}) \ (\langle T_e \rangle - \langle T_i \rangle) / \langle T_e \rangle^{3/2},$$

with q_{ei} the collisional power density transfer from electrons to ions, $\langle T \rangle$ the volume average temperature and $ln\Lambda$ the Coulomb logarithm. The resistive diffusion time τ_R is estimated by the Spitzer resistivity η_S with an approximate neoclassical correction [22]: $\tau_R = \mu_0 a^2/\langle \eta_S \rangle \times \langle [1-(r/R_0)^{0.5}]^2 \rangle$. To formalize τ_θ , we refer to the analysis presented in [23], showing that after few ion collision times τ_i , with $\tau_i \propto 1$

To formalize τ_{θ} , we refer to the analysis presented in [23], showing that after few ion collision times τ_{i} , with $\tau_{i} \propto \langle T_{i}^{3/2} \rangle / n_{e}$, the decay of the poloidal flow has an exponential trend with the characteristic time $\tau_{\theta} = 0.507\tau_{i}/ln(2)$.

The spontaneous rotation in ohmic tokamak discharges is discussed in [24] for TCV experiments. The velocity common to ions and electrons, namely the single-fluid velocity modelled in (4), (5), is due to the electric drift. In [24] the toroidal component of this velocity is found to be a multiple (~3) of the neoclassical ion diamagnetic velocity, approximately given by $(dT_i/dr)/(eB_\theta)$, with e the electron charge magnitude. In RFX-locking the unperturbed value of Ω_{ϕ} at the resonant surface (i.e. the steady-state value in the absence of EF, implying $\partial/\partial t = 0$, $T_{EM,\phi} = 0$) is set according to this observation: $\Omega_{\phi}(r_{mn}) = 3 (dT_i/dr)/(eB_{\theta}R_0)]_{r=r_{mn}}$. This fixes the radially constant source S_{ϕ} . The unperturbed profile of Ω_{θ} is then computed from (5) with $\partial/\partial t = 0$, $T_{EM,\theta} = 0$, under the assumption $S_{\theta} = S_{\phi}$.

3. SIMULATIONS

In this section we discuss dynamical simulations of the penetration of a m=2, n=1 EF. First, we set the geometrical parameters of the machine, the time constant of the passive structures, and the characteristics of the coils grid. The latter are required to define the term $L_c^{m,n}$ which enters equation (15), but they are irrelevant for the outcome of the simulation. Then, we fix the magnetic equilibrium. In cylindrical geometry is not easy finding m=2, n=1 tearing-stable equilibria. Here, we accomplish this by taking $q(0)=0.7, q(a)\approx 3$, with q(r) the cylindrical safety factor. Finally, we set the toroidal magnetic field magnitude, the plasma density, and we take $Z_{eff} = A_i = 1$. This completely defines the kinetic quantities defined in paragraph 2.4. After 0.2s of simulation, we apply the EF by the coils' current harmonic $I_c^{2,1}$, imposing a linearly increasing amplitude of the same. The EF amplitude is quantified by the radial field absolute value at the plasma facing structure, namely at the vacuum vessel: $|b_r(r_v)|$. Note that, $b_r(r_v)$ is total radial field, summing up the plasma, passive structures and coils contributions. The frequency ω (see definition in paragraph 2.2) decreases owing to the EM torque (6), until it reaches a complete stop at a given critical value of the EF amplitude: this mark the EF penetration. Examples of this process are given in figure 1 for a cylindrical proxy of JET ($R_0 = 3$, a = 1, $r_v = 1.3$, b = 1.7, $\tau_v = 3 \times 1.7$ 10^{-3} , $\tau_b=3\times10^{-2}$ in SI units) and a cylindrical proxy of RFX-mod2 ($R_0=2$, a=0.4965, $r_v=0.5125$, $b=10^{-2}$ 0.55, $\tau_v = 0.1$, $\tau_b = 2.4 \times 10^{-2}$ in SI units). The significant difference of the EF threshold in the two cases is explained by the different density, toroidal field and plasma-vessel distance taken in the simulations of the two devices.

A unified description of the EF penetration in the two devices is now presented. According to equation (77) of [5], the EF amplitude threshold obtained with a full stationary model is expressed in terms of the normalized total radial field at the vacuum vessel $|b_r(r_v)|_{thr}/B_{\phi}$ times the factor $r_v E_{vs}/r_{m,n}$ which compensates for the plasmavessel proximity dependence of $|b_r(r_v)|$. Therefore, that equation suggests using the metric $|b_r(r_v)|_{thr}/B_{\phi} \times r_v E_{vs}/r_{m,n}$ to express the EF threshold. We run several simulations by performing a scan in density and toroidal field. In the JET case we also perform a size scaling by considering besides the actual geometry $(R_0 = 3)$ two hypothetical further cases, $R_0 = 4$, $R_0 = 1.5$, with the other lengths varied in proportion. Then we take a multivariate regression of the EF penetration threshold with the scan parameters. The result is the following:

23)
$$RFXmod2 \rightarrow |b_r(r_v)|_{thr}/B_\phi \times r_v E_{vs}/r_{m,n} = 9.5 \times 10^{-4} n_e^{1.13 \pm 0.01} B_\phi^{-1.54 \pm 0.03}$$

24)
$$JET(R_0=3) \rightarrow |b_r(r_v)|_{thr}/B_\phi \times r_v \; E_{vs}/r_{m,n} = 9.6 \times 10^{-4} n_e^{0.98 \pm 0.01} B_\phi^{-1.48 \pm 0.02}$$

$$25) \ \ JET(R_0=1.5,3,4) \ \rightarrow \ |b_r(r_v)|_{thr}/B_\phi \times r_v \ E_{vs}/r_{m,n} = 7.7 \times 10^{-4} n_e^{1.00\pm0.01} B_\phi^{-1.49\pm0.02} R_0^{0.19\pm0.02}$$

26)
$$JET(R_0=1.5,3,4) \rightarrow |b_r(r_v)|_{thr}/B_\phi=2.7\times 10^{-4}n_e^{1.00\pm0.01}B_\phi^{-1.49\pm0.02}R_0^{0.19\pm0.02}$$

In the above expressions n_e is given in $10^{19}m^{-3}$ units. Regression (24) refers to the actual JET size, whereas (25) includes the size scaling so it contains R_0 as additional parameter. Regression (26) discards the r_v $E_{vs}/r_{m,n}$ term, so it differs from (25) only by a global factor. As shown in figure 2 the quality of the fits (23), (24), (25) is very good. Moreover, scaling laws (25) aligns almost perfectly the RFXmod2 and JET simulated thresholds, despite the different layout of the two devices, whereas (26) does not: see figure 3. Therefore, only the metric $|b_r(r_v)|_{thr}/B_\phi \times r_v$ $E_{vs}/r_{m,n}$ provides a unified picture of the phenomenon. Expression (25) also confirms, with full dynamical simulations, the steady-state result of [6]. The size dependence in (25) is not strong, but the scaling with R_0 is clearly positive. As explained in [6] this result is obtained thanks to the equality $\tau_M = \tau'_{Ei}$, whereas the more customary assumption $\tau_M = \tau_E$, with τ_E the total energy confinement time, leads to a negative scaling with R_0 in ohmic conditions. Experimentally, this is the most difficult dependence to be assessed. As discussed in [25], the scaling with R_0 is positive, and the exponent should be about 0.2 (the exponent 1.4 obtained in one of the regressions presented in [25] is doubtful according to the authors). The density and toroidal field exponents are in good agreement with the result of [25]. Expression (24) is also quite close to the scaling $|b_r|_{thr}/B_\phi \propto n_e^{0.94\pm0.06}B_\phi^{-1.2\pm0.05}$ obtained in JET discharges [26].

The analysis just discussed highlights $|b_r(r_v)|_{thr}/B_\phi \times r_v E_{vs}/r_{m,n}$ as a metric able to unify experiments with different layout. In other words, it can be used to extrapolate, within a cylindrical approximation, the experimental EF threshold data obtained in one device to any other device. Of course, in this extrapolation a dependence R_0^α with $\alpha \approx 0.2$ needs to be included to account for the different machine sizes. To this purpose, RFX-mod2 [10,

11] operated as a tokamak will be particularly suitable to perform EF penetration studies for several reasons. First, RFX-mod2 benefits of a close-fitting stabilizing shell, which should make the tokamak plasma stable to tearing modes, the ideal condition to perform this study. Second, the full coverage of the torus by active coils and the circular cross section of the device allow the application of EF with quite pure helicity, net of the toroidal coupling which unavoidably enriches the content of poloidal mode numbers m. Moreover, plasma with different shapes, from the circular to the X-point can be realized by the field shaping coils system. Finally, the large number of magnetic sensors allows a precise detection of the phenomenon. The results, expressed in term of the above universal metric, will be useful to make extrapolations to other machines not yet in operations.

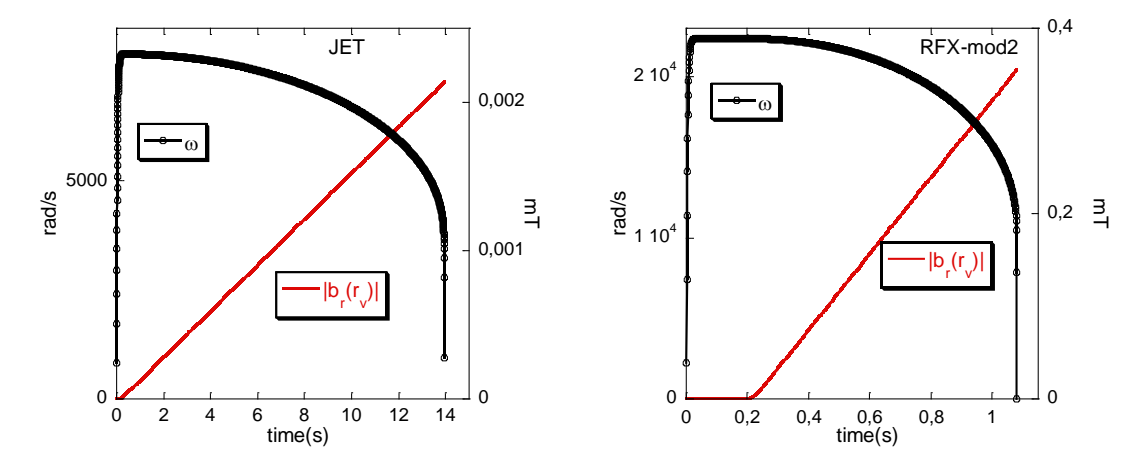


FIG. 1. Dynamical simulation of the EF penetration for JET (left) and RFXmod2 (right). In the JET case we take $n_e = 10^{20} m^{-3}$, $B_{\phi} = 2.2T$. In the RFXmod2 case we take $n_e = 1.3 \times 10^{19} m^{-3}$, $B_{\phi} = 0.5T$. EF penetration corresponds to the instant where ω drops to zero.

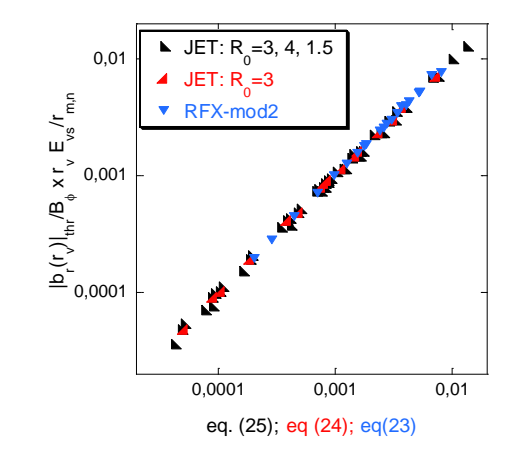


FIG. 2. EF penetration threshold in terms of $|b_r(r_v)|_{thr}/B_{\phi} \times r_v E_{vs}/r_{m,n}$ as function of scaling laws (23) for RFXmod2, (24) for JET, and (25) for JET with size scaling

4. CONCLUSIONS

Simulations of EF penetration have been carried out for cylindrical proxy of JET and RFX-mod2. This has been accomplished by the RFX-locking code, already used to simulate the tearing mode dynamic [9], with the inclusion of recently developed specific physics to model the linear plasma response to a resonant EF [5]. The results confirm previous theoretical analysis [6] and are in good agreement with experimental scaling laws [25, 26]. We also propose to express the EF threshold in a metric able to unify machines with different front-end systems: indeed the predictions for JET and RFX-mod2 superimpose almost exactly in this metric (figure 3, left). This metric will be important to extrapolate the results of the next EF penetration experiments planned on RFX-mod2. Finally, we give an estimate of the EF threshold expected in the ohmic ITER plasma on the basis of (25): by taking $R_0 = 6.2m$, $B_{\phi} = 5.3T$, $n_e = 10^{20}m^{-3}$, q(a) = 3.3, $r_{m,n}/r_v = 0.7$, $E_{vs} = 2$, one gets $|b_r(r_v)|_{thr}/B_{\phi} \cong 3 \times 10^{-3}$

IAEA-CN-316/INDICO ID

 10^{-4} , which is significantly larger that the EF normalized value $\cong 5 \times 10^{-5}$ expected after correction with the Error Field Correction Coils [27].

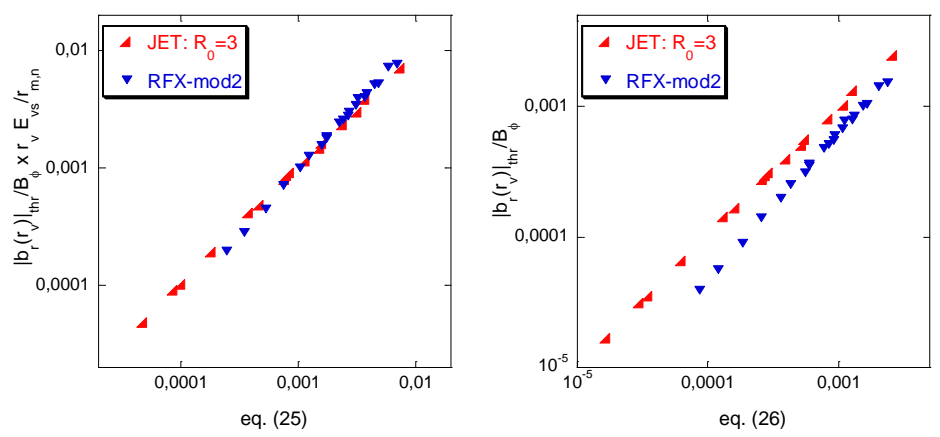


FIG. 3. EF penetration threshold in terms of $|b_r(r_v)|_{thr}/B_{\phi} \times r_v E_{vs}/r_{m,n}$ as function of scaling law (25)(left), and in terms of $|b_r(r_v)|_{thr}/B_{\phi}$ as function of scaling law (26)(right) for RFXmod2 and for JET,

REFERENCES

- [1] R. FITZPATRICK, Nucl. Fusion 33 1049 (1993).
- [2] A. COLE, R. FITZPATRICK, Phys. Plasmas 13 032503 (2006)
- [3] JONG-KYU PARK, Phys. Plasmas 29 072506 (2022)
- [4] R. FITZPATRICK, Physics of Plasmas 29 032507 (2022)
- [5] P. ZANCA, Nucl. Fusion 65 056023 (2025)
- [6] P. ZANCA, submitted to Plasma Physics and Controlled Fusion (2025)
- [7] P ZANCA, Plasma Phys. Control. Fusion **51** 015006 (2009)
- [8] P. ZANCA et al, Nucl. Fusion **55** 043020 (2015).
- [9] L. PIRON et al, Nucl. Fusion **64** 066029 (2024).
- [10] D. TERRANOVA et al, Nucl. Fusion 64 076003 (2024)
- [11] L. MARRELLI et al, Nucl. Fusion 59 076027 (2024)
- [12] R. FITZPATRICK, Phys. Plasmas 30 042514 (2023)
- [13] R. FITZPATRICK, Phys. Plasmas 6 1168 (1999)
- [14] H.P. FURTH et al, Physics of Fluids 6 459 (1963)
- [15] I. S. GRADSHTEYN, I. M. RYZHIK, Table of Integrals, Series, and Products, 7th edition (edited by Alan Jeffrey and Daniel Zwillinger, 2007)
- [16] C. G. GIMBLETT, Nucl. Fusion 26 617 (1986)
- [17] P. ZANCA, Plasma Phys. Control. Fusion 52 115002 (2010)
- [18] W. PFEIFFER, R. E. WALTZ, Nuclear Fusion 19 51 (1979)
- [19] EQUIPE TFR, Nuclear Fusion 16 279 (1976)
- [20] L.A. ARTSIMOVITCH, Nuclear Fusion 12 216 (1972)
- [21] P. C. DE VRIES et al, Plasma Phys. Control. Fusion 48 1693 (2006)
- [22] J.A. WESSON, 'Tokamaks' 3rd edition (Oxford: Clarendon) (2004)
- [23] R. C. MORRIS et al, Phys. Plasmas 3 (12) 4513 (1996)
- [24] A. SCARABOSIO et al, Plasma Phys. Control. Fusion 48 663 (2006)
- [25] N.C. LOGAN et al, Nuclear Fusion 60 086010 (2020)
- [26] R.J. BUTTERY et al, Nucl. Fusion 39 1827 (2024)
- [27] V.M. AMOSKOV et al, Physics of Particles and Nuclei Letters 12 No. 3, 375 (2015)